A Practical Approach to Diagnosis of Spinal Dysraphism

Bárbara Trapp, MD
Tomás de Andrade Lourenção Freddi, MD
Monique de Oliveira Morais Hans, MD
Isadora Fonseca Teixeira Lemos Calixto, MD
Emi Fujino, MD
Laila Cristina Alves Rojas, MD
Stênio Burlin, MD
Danilo Manuel Cerqueira Costa, MD, MSc
Henrique Carrete Junior, MD, PhD
Nitamar Abdala, MD, PhD
Luís Antônio Tobaru Tibana, MD
Eduardo Takashi Takehara, MD
Gustavo Dalul Gomez, MD

Spinal dysraphisms (SDs) are congenital malformations of the spinal cord, determined by derangement in the complex cascade of embryologic events involved in spinal development. They represent a heterogeneous group ranging from mild clinical manifestations—going unnoticed or being discovered at clinical examination—to a causal factor of life quality impairment, especially when associated with musculoskeletal, gastrointestinal, genitourinary, or respiratory system malformations. Knowledge of the normal embryologic development of the spinal cord—which encompasses three main steps (gastrulation, primary neurulation, and secondary neurulation)—is crucial for understanding the pathogenesis, neuroradiologic scenarios, and clinical-radiologic classification of congenital malformations of the spinal cord. SDs can be divided with clinical examination or neuroradiologic study into two major groups: open SDs and closed SDs. Congenital malformations of the spinal cord include a wide range of abnormalities that vary considerably in imaging and clinical characteristics and complexity and therefore may represent a diagnostic challenge, even for the experienced radiologist.

Online supplemental material is available for this article.

Abbreviations: CSF = cerebrospinal fluid, SD = spinal dysraphism

RadioGraphics 2021; 41:0000–0000

https://doi.org/10.1148/rg.2021200103

Content Codes: MR NR PD

From the Department of Diagnostic Imaging, Division of Neuroradiology, Universidade Federal de São Paulo (UNIFESP), Rua Napoleão de Barros 800, São Paulo SP 04024-002, Brazil (B.T., M.d.O.M.H., I.F.T.L.C., E.F., L.C.A.R., S.B., D.M.C.C., H.C.J., N.A., L.A.T.T., E.T.T., G.D.G.); Department of Diagnostic Imaging, Division of Neuroradiology, Hospital do Coração (HCor), São Paulo, Brazil (T.d.A.L.F.); and Department of Diagnostic Imaging, Division of Neuroradiology, Fundação Instituto de Pesquisa e Estudo de Diagnóstico por Imagem (FIDI), São Paulo, Brazil (B.T., M.d.O.M.H., I.F.T.L.C., L.C.A.R., S.B., L.A.T.T.). Presented as an education exhibit at the 2019 RSNA Annual Meeting. Received May 1, 2020; revision requested June 18 and received July 12; accepted July 27. For this journal-based SA-CME activity, the authors, editor, and reviewers have disclosed no relevant relationships. **Address correspondence to** G.D.G. (e-mail: *gdalulgomez@gmail.com*).

SA-CME LEARNING OBJECTIVES

After completing this journal-based SA-CME activity, participants will be able to:

- Understand the embryologic steps of normal spine development and describe the main embryologic derangements that lead to each type of SD.
- Discuss the proper radiologic classification of each SD.
- Recognize the main MRI findings that constitute and differentiate each group of congenital malformations of the spinal cord.

See rsna.org/learning-center-rg.

Introduction

Congenital malformations of the spine and spinal cord are generally described under the umbrella term *spinal dysraphisms* (SDs). The etymologic origin of the term *dysraphism* is from the Greek words *dys* (bad) and *rhaphḗ* (suture); therefore, it should be applied only to primary neurulation abnormalities. However, in medical practice, it is used to describe a diverse group of abnormalities of spinal cord development that occur between the 2nd and 6th gestational weeks and show incomplete midline closure of mesenchymal, osseous, and nervous tissue (1).

Neural tube defects are the second most common type of birth anomaly after congenital heart disease (2). SDs are a subtype of neural tube defects, with an estimated prevalence of about one to three per 1000 live births (3). The lumbosacral spine is the most

TEACHING POINTS

- Neuroimaging plays a critical role in diagnosis, detection of associated malformations, therapeutic planning, and postoperative evaluation of SDs. In general, SDs are best characterized with MRI, since it provides excellent spatial resolution and increased tissue contrast and does not involve ionizing radiation.
- According to the clinical-radiologic classification, SDs are categorized into two major groups: open SDs and closed SDs, depending on whether there is a skin defect overlying the abnormality. In open SDs, there is direct exposure of the neural tissue and meninges to the external environment. In closed SDs, the neural and meningeal tissues are covered by skin or subcutaneous tissue; therefore, there is no exposure of the placode.
- Myelomeningocele is a neurosurgical emergency—like all open SDs—and represents the most common form of open SD, accounting for more than 98% of cases. It has a prevalence of approximately 0.6–1.0 per 1000 live births, and females are affected slightly more often than males.
- Lipomas with dural defect (LDDs) constitute a continuum of abnormalities (lipomyelomeningocele, lipomyelocele, and lipomyeloschisis) that share a common pathophysiologic process. They differ from each other by the position of the cord-lipoma interface, which is important information for the surgical approach. Together, these anomalies represent 75.9% of all spinal lipomas and 16.4% of all closed SDs.
- Differentiation between the two types of diastematomyelia depends on development of primitive streak tissue. In type I, the intervening primitive streak develops into bone or cartilage, creating a septum (radiologic mark) that separates the dural sac in two. In type II, the primitive streak is reabsorbed or forms a fibrous septum, with a single dural sac involving both hemicords.

common site, involved in 90% of cases, followed by the thoracic spine (6%–8%) and cervical spine (2%–4%) (4). Antenatal care and maternal nutrition play a central role in adequate fetal spine development; thus, the worldwide prevalence of SD may vary depending on the socioeconomic conditions in each country.

As a result of the close embryologic relationship between the caudal cell mass—which originates in the lumbosacral spine—and the cloaca, spinal malformations caused by secondary neurulation failures are frequently found in association with anorectal or urogenital anomalies (1,5). Furthermore, as the notochord has an important role in formation of the neural tube, as well as thoracic and abdominal viscera, these patients often have anomalies of the upper gastrointestinal tract or respiratory tract (1). Ultimately, systemic conditions manifesting with vertebral anomalies—such as VACTERL (*v*ertebral, *a*norectal, *c*ardiac, *t*racheal, *e*sophageal, *r*enal, and *l*imb anomalies) syndrome or Klippel-Feil syndrome—should be investigated for spinal cord malformations, given that vertebral column formation is closely influenced by many of the same factors that influence development of the spinal cord (1).

Detailed knowledge of spinal cord embryology and the key imaging findings of SDs is essential for the radiologist, who plays a critical role in diagnosis of these conditions. Early detection of SD is related to better outcome, since it allows parent counseling and appropriate treatment decisions, minimizing the morbidity inherent to these malformations.

Etiology

SDs are a group of developmental disorders with multifactorial etiology, comprising genetic, environmental, and nutritional components (6,7).

Genetic factors are probably among the most important contributing to spine developmental errors. However, despite major advances in neurogenetics over the past 10 years, little is still known of normal and abnormal spinal development. Most published studies were based on small case series and do not show statistically significant results in humans (1,7). Variations in some specific genes have been related to development of SD, such as *MTHFR*, *MTHFD1*, *MTRR*, *VANGL1*, *VANGL2*, *CELSR1*, and *FUZ*, as well as variants in the T locus on chromosome 6q (2).

Genes encoding proteins that participate in folate one-carbon metabolism have been broadly investigated, owing to the potential role of folic acid in preventing SD. The methylenetetrahydrofolate reductase *(MTHFR)* gene is the most studied, and its C677T variant is the most accepted genetic factor linked to human SD; however, this association is seen only in certain populations (non-Hispanic origin) (8). Currently, there are no reliable genes or genetic counseling available for detecting human SD; thus, larger controlled studies are necessary to demonstrate this relationship.

Periconception environmental factors—including maternal obesity, poor nutrition, tobacco exposure, hyperhomocysteinemia, sedentarism, and mental stress—play a central role in this process, given its relation to excessive oxidative stress and inflammation, which accelerate maternal biologic aging through faster telomere shortening (6). There is evidence of higher incidence of SD in embryonic mice with shorter telomeres, and some authors have hypothesized that this theory could be extrapolated to humans (6).

One of the most notable environmental factors implicated in the occurrence of SD is periconception maternal nutrition, which is closely related to the socioeconomic condition of the patient. In this scenario, folic acid deficiency is one of the most remarkable factors (9). Some authors have suggested that folic acid may play a central role in preventing SD. It is a natural antioxidant and in high doses can correct defects in homocysteine metabolism (10,11).

A European meta-analysis suggested that folic acid supplementation with 4 mg daily should be initiated 5–6 months before conception (10). This prophylactic scheme leads to optimal red blood cell folate levels and reduces the risk of SD occurrence in the offspring (10). Other nutrient deficiencies that may be involved in this process include inositol, vitamin B_{12}, choline, retinoic acid, and iron (12).

Normal Embryology of Spinal Cord

Development of the spine and spinal cord is a highly coordinated and complex process consisting of several consecutive steps that can be summarized in three basic embryologic stages: gastrulation, primary neurulation, and secondary neurulation.

Gastrulation

Gastrulation is defined by transformation of the bilaminar embryonic disk into a trilaminar embryonic disk through addition of a third interposed layer—the mesoderm (3,13,14). At this stage, the notochord also forms. Its formation begins between the 2nd and 3rd gestational weeks and ends in the middle of the 3rd gestational week (13,15).

In the initial process of gastrulation, the embryo is formed by a bilaminar embryonic disk. This is a flat almost circular disk, composed of two distinct cell layers: the epiblast and hypoblast. The thickest layer is formed by the epiblast (also known as primitive ectoderm), which consists of tall columnar cells related to the amniotic cavity. The hypoblast forms another layer, thinner and consisting of small cuboidal cells adjacent to the exocoelomic cavity (yolk sac) (3).

The cells of the epiblast migrate ventrally and extend along the disk for about half its length to form the primitive streak. At one end of the primitive streak, a nodular rapidly proliferating group of cells known as the primitive node of Hensen is formed, which defines the cephalic end of the embryo (3,13,14,16). At this point, cells migrate through a primitive pit between the epiblast and hypoblast and displace the hypoblast caudally to form the endoderm (3,13–16). Continuous waves of migrating cells travel bilaterally above the endoderm to form the mesoderm. The notochord is formed from mesoderm cells that migrate along the midline to form this malleable rod-shaped structure along the embryonic craniocaudal axis (Fig 1) (3,13,15,16).

Primary Neurulation

Primary neurulation extends during weeks 3 and 4 of gestation (13,15), starting with formation of the neural plaque in the ectoderm and ending with closure of the neural tube in the mesoderm. The notochord induces formation of the neural plate in the dorsal midline of the ectoderm, cephalic to the Hensen node. The neural groove in the center and the two neural folds (one on each side) are formed when the neural plate attaches to the notochord and starts bending, at the level of the ventral hinge point.

The neural folds progressively increase in size and flex to approach each other, until they eventually fuse in the midline to form the neural tube. It then closes bidirectionally in a zipperlike manner, starting at the rhombencephalon and proceeding both cephalically and caudally. With the detachment on both sides of the neuroectoderm, the cutaneous ectoderm seals the overlying skin (3,13,14,16) (Fig 2).

Secondary Neurulation

Secondary neurulation—the last embryologic step—begins at the end of primary neurulation and occurs during weeks 5 and 6 of gestation (13,15). At this stage, an additional part of the neural tube is formed caudal to the primary neural tube. A solid mass of totipotential cells forms the tail bud, which subsequently undergoes internal cavitation. This forms the secondary neural tube.

The secondary neural tube merges with the cranial neural tube, which was formed by primary neurulation, giving rise to a continuous structure (Fig 3) (13,16). Then, through a process called retrogressive differentiation, the tail bud regresses to form the tip of the conus medullaris and the filum terminale (3,14–16). Abnormalities in any of these steps can lead to spine or spinal cord malformations.

Role of Neuroimaging in Diagnosis of SDs

Neuroimaging plays a critical role in diagnosis, detection of associated malformations, therapeutic planning, and postoperative evaluation of SDs. In general, SDs are best characterized with MRI, since it provides excellent spatial resolution and increased tissue contrast and does not involve ionizing radiation. In this scenario, imaging at high field strength of 1.5 T or greater is preferred.

A targeted MRI protocol is essential for optimal visualization of SDs, correct vertebral numbering, and depiction of associated malformations. It should always include at least high-resolution sagittal T1- and T2-weighted images of the whole spine and one panoramic coronal sequence (3). Dedicated axial T1- and T2-weighted images of the specific region of interest using section thickness of 3.0 mm or less are also recommended (3).

In addition, high-resolution heavily T2-weighted images can enrich evaluation of SD, as

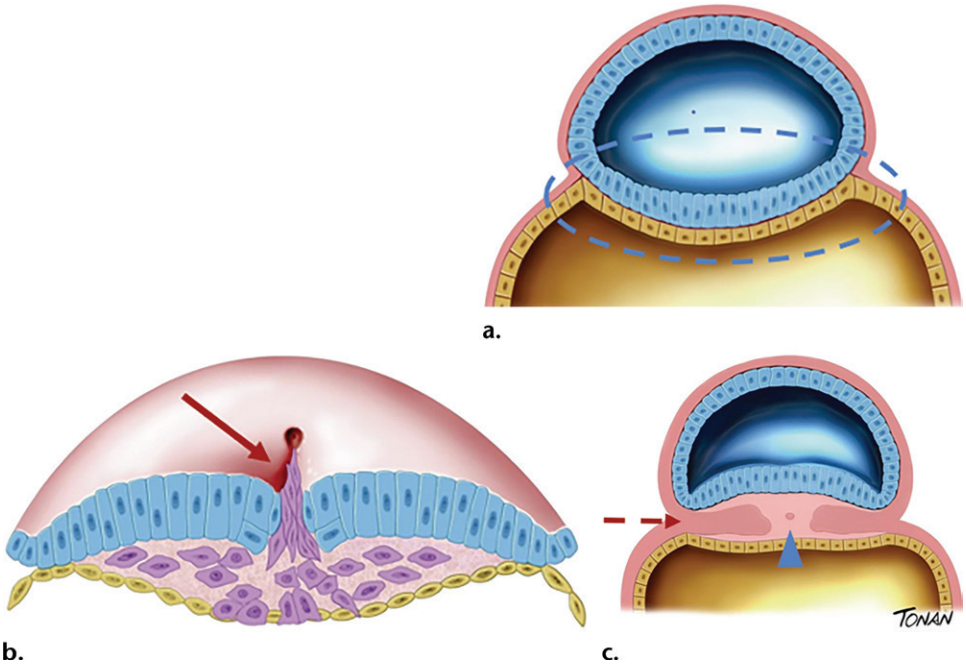

Figure 1. Gastrulation. **(a)** Bilaminar embryonic disk (blue dashed oval) composed of layers of the hypoblast (yellow cells)—with edges facing the yolk sac—and the ectoblast (blue cells), with edges facing the amniotic sac. **(b)** Cells (purple cells) migrate through a primitive pit (arrow) between the epiblast (blue cells) and hypoblast (yellow cells) and displace the hypoblast caudally to form the endoderm. **(c)** Continuous waves of migrating cells travel bilaterally above the endoderm to form the mesoderm (arrow) and notochord (arrowhead), which is formed from mesoderm cells. Now the embryo is composed of a trilaminar disk and has the notochord fully formed.

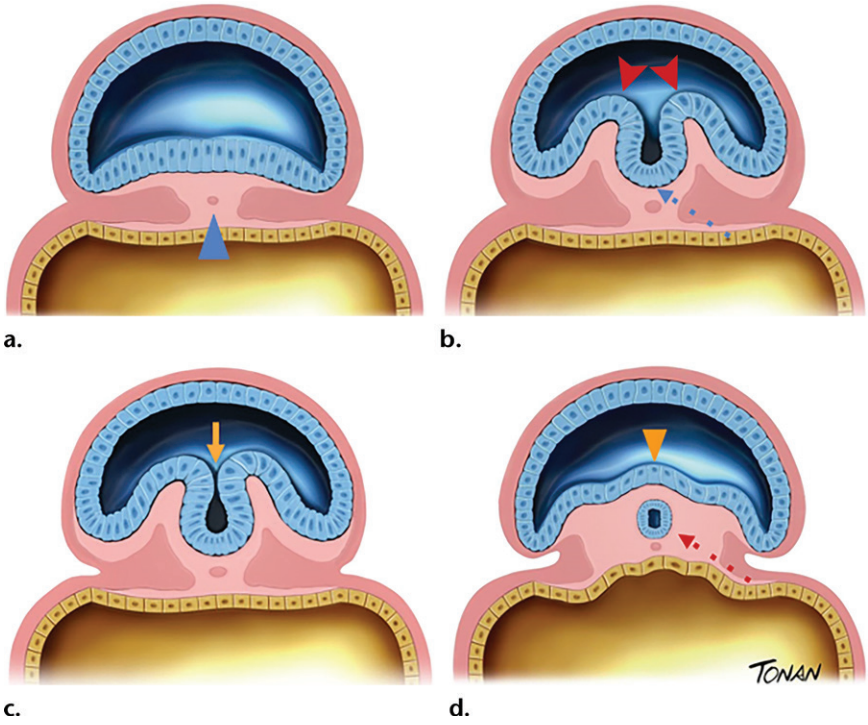

Figure 2. Primary neurulation. **(a)** The notochord (arrowhead) induces formation of the neural plate (blue cells) in the dorsal midline of the ectoderm. **(b)** The neural groove in the center (arrow) and the two neural folds (one on each side) (arrowheads) are formed and start bending. **(c)** The neural folds progressively increase in size and flex to approach each other, until they fuse in the midline (arrow). **(d)** The neuroectoderm detaches on both sides from the cutaneous ectoderm, forming the neural tube (arrow) in the mesoderm, which then closes bidirectionally in a zipperlike manner. Then, the cutaneous ectoderm seals the overlying skin (arrowhead).

they provide higher spatial resolution (3). However, this sequence requires patient cooperation, which is hampered by the age group involved and associated poor health conditions. In situations where MRI is essential but patient cooperation is lacking, use of sedation may be necessary to obtain adequate images (3).

Other imaging methods usually play a secondary role in evaluation of SD. US is often used in the neonatal period, when the degree of spinal

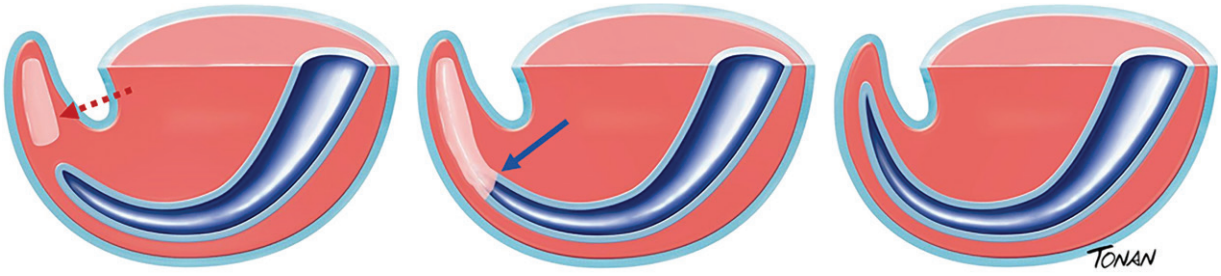

a. b. c.

Figure 3. Secondary neurulation. **(a)** A solid mass of totipotential cells (arrow) forms the tail bud. **(b)** The tail bud cavitates internally (central white line), forming the secondary neural tube, which merges cranially (arrow) with the neural tube, previously formed by primary neurulation. **(c)** Therefore, this merger gives rise to a continuous and centrally cavitated structure.

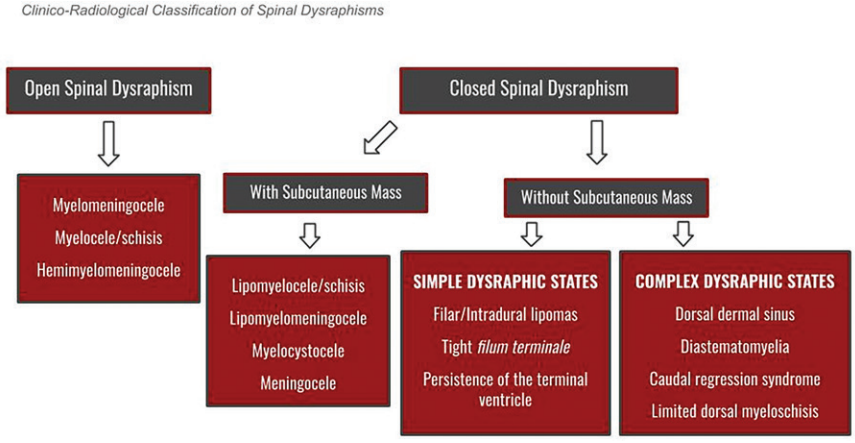

Figure 4. Clinical-radiologic classification of SDs.

ossification is still incomplete, facilitating passage of sound waves and allowing better definition of neurologic structures. Furthermore, US does not involve exposure to ionizing radiation and enables assessment of associated malformations, such as genitourinary anomalies. However, it is not indicated for evaluating open SDs in the postnatal period owing to patient predisposition to infections.

CT has a limited role in evaluation of SD given its low sensitivity, poor tissue contrast, and exposure to ionizing radiation. It should be used only in selected cases, such as in severe bone anomalies (3) or when patient sedation is impossible.

Classification of SDs

The most used classification of SDs involves a practical approach using a combination of clinical and radiologic factors, which help restrict the scope of the differential diagnosis (17). According to the clinical-radiologic classification (Fig 4), SDs are categorized into two major groups: open SDs and closed SDs, depending on whether there is a skin defect overlying the abnormality. In open SDs, there is direct exposure of the neural tissue and meninges to the external environment.

In closed SDs, the neural and meningeal tissues are covered by skin or subcutaneous tissue; therefore, there is no exposure of the placode (18). Closed SDs are subdivided into two groups: those with a subcutaneous mass (eg, lipomas with a dorsal defect and meningocele) and those without a subcutaneous mass (eg, intradural lipoma). Closed SDs lacking a subcutaneous mass can be further classified as simple dysraphic states (eg, persistent terminal ventricle) and complex dysraphic states (eg, diastematomyelia and caudal regression syndrome [CRS]) (1,19–21).

In addition to the clinical-radiologic approach, neuroradiologists must have knowledge of spinal embryology to make a precise diagnosis. Embryologic classifications (Table 1) are primarily based on correlation of imaging findings with the corresponding derangement in the complex cascade of embryologic events (18).

Open SDs

Myelomeningocele

Myelomeningocele is clinically and radiologically defined by two main characteristics: *(a)* exposure of the neural placode to the environment with *(b)* expansion of the underlying subarachnoid space. Both protrude through the spina bifida, with elevation of the placode above the skin surface by expansion of the subarachnoid space in the midline of the back (Fig 5) (1,3,17).

Table 1: Embryologic Classification of SDs

Step of Embryologic Derangement	Resultant Abnormalities
Gastrulation (2–3 weeks gestation)	Diastematomyelia,* caudal regression syndrome,† segmental spinal dysgenesis
Primary neurulation (3–4 weeks gestation)	Myelomeningocele, myelocele/myeloschisis, hemimyelomeningocele, nonterminal myelocystocele, meningocele, lipomyelomeningocele, lipomyelocele/lipomyeloschisis, intradural lipoma, dermal sinus, limited dorsal myeloschisis
Secondary neurulation (4–6 weeks gestation)	Terminal myelocystocele, persistent terminal ventricle, filar cyst, tight filum terminale, filum terminale lipoma, persistent secondary neural tube

*Disorder of midline notochordal integration.
†Disorder of notochordal formation.

Myelomeningocele is a neurosurgical emergency—like all open SDs—and represents the most common form of open SD, accounting for more than 98% of cases. It has a prevalence of approximately 0.6–1.0 per 1000 live births (1,3,17), and females are affected slightly more often than males (1). The lower lumbar and upper sacral regions are the most frequently compromised segments, corresponding to approximately 80%–98% of cases. Myelomeningocele is rare in the cervical and upper thoracic spine.

Fortunately, there is a reduction in myelomeningocele cases owing to a supplemental diet of folic acid before and during pregnancy. Incredible advances in corrective intrauterine surgery have further reduced the degree of neurologic injury.

There are two main theories regarding the embryologic pathophysiology of open SD: one is represented by a primary failure to close the neural tube, while the other supports the reopening of the already closed neural tube (13). The first theory, which encompasses the defect in primary neurulation, is probably more appropriate to explain an open spinal cord defect in humans (1,3,17). A segment of neural plate remains frozen in its primordial stage, not evolving to formation of the neural folds and neural groove, giving rise to the placode (open neural tube). The unfused edges of the adjacent cutaneous ectoderm remain attached to the nonneurulated neural plate segment and fail to form the future skin, explaining the resultant midline skin defect (1,3,14,17).

The outer surface of the placode represents what would be the future spinal cord ependymal surface and is directly visible at physical inspection. The inner surface of the placode represents what would be the outer layer of the spinal cord where nerve roots originate (1,17). Migration of the mesenchyme behind the neural tube is prevented owing to a failure to separate the neuroectoderm from the adjacent ectoderm, causing a defect in the musculoskeletal structures (13,22,23).

The neurologic deficit in open SD is explained by the malformation itself and by the exposure of the nonneurulated neural tissue (placode) to the environment, suffering physical trauma and chemical injury due to the abrasive effect of the amniotic fluid (1,3,17). The clinical spectrum depends on the spinal cord segment involved and the extent and severity of damage to the placode. Since the lumbosacral segment is the most affected, the clinical picture usually includes deficits of the lower extremities, paraplegia, bowel and bladder incontinence, sexual dysfunction, skeletal deformities, hindbrain dysfunction, and intellectual and psychological disturbances (1,3,17).

It is rare to perform MRI in newborns with open SD because the diagnosis is usually made with obstetric US and confirmed with visual inspection postnatally. Thereafter, fetal MRI is the modality of choice for evaluating these patients, as it has higher spatial and contrast resolution. To best accomplish evaluation of the fetal central nervous system, it is recommended to perform MRI after the 20th gestational week. Fetal MRI of untreated myelomeningocele shows discontinuity of skin and subcutaneous tissue (subcutaneous fat, fascia, muscle, and bone), a placode exposed to the environment, and an expanded and herniated cerebrospinal fluid (CSF) space through the defect (meningocele). The spinal cord entering the meningocele and anchoring to the placode may also be depicted (Fig 5) (1,3,17).

Postnatal MRI of untreated myelomeningocele may show the nerve roots that originate from the ventral surface of the placode and course anteriorly through the meningocele and into the dilated subarachnoid spaces of the spinal canal, going to the neural foramina (1,3,17).

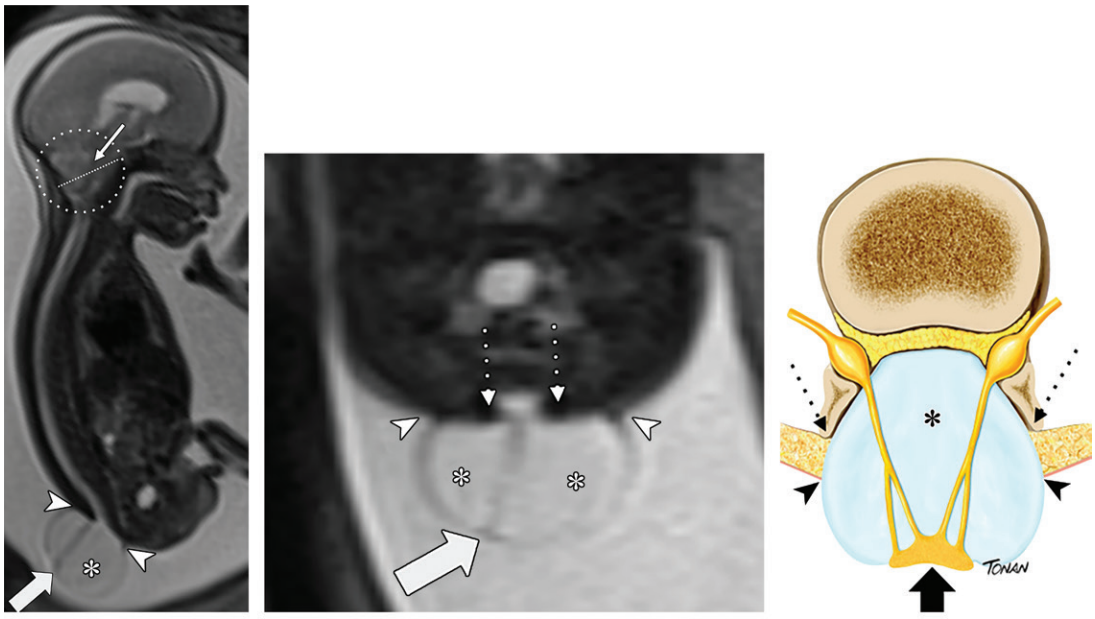

Figure 5. Myelomeningocele with Chiari II malformation. **(a, b)** Sagittal **(a)** and axial oblique **(b)** single-shot fast spin-echo T2-weighted MR images of the fetal central nervous system show discontinuity of skin and subcutaneous tissue (arrowheads) in the lumbosacral region with herniation of nervous tissue through the spina bifida (thin arrows in **b**), forming the placode, which is exposed to the amniotic fluid (thick arrow). There is expansion of the adjacent subarachnoid space (*). Chiari II malformation is characterized by a small posterior fossa (dotted white circle in **a**), a slitlike fourth ventricle (thin arrow in **a**), and herniation of the cerebellar tonsils or vermis through the foramen magnum (dotted white line in **a**). **(c)** Drawing shows discontinuity of skin and subcutaneous tissue (arrowheads), with the placode exposed to the environment and elevated above the skin surface (thick arrow) by expansion of the underlying subarachnoid space (meningocele) (*), both herniated through the spina bifida (thin arrows).

Myelocele and Myeloschisis

Myelocele represents a rarer form of open SD in which the placode is exposed to the environment through a spina bifida, like in myelomeningocele, but without posterior expansion of the subarachnoid space (meningocele) (1,3,17). The embryology and clinical aspects, including the association with Chiari II malformation, are equivalent to those of myelomeningocele (1,3,13,14,16,17,23,24).

The MRI findings are similar to those described in myelomeningocele, but without the meningocele. There is discontinuity of skin and subcutaneous tissue, with the placode exposed to the environment and forming the posterior wall of the spina bifida. The placode is flush with the skin surface (myelocele) or depressed (myeloschisis) because there is no expansion of the underlying subarachnoid space. The affected spinal cord segment anchors in the ventral wall of the placode (Fig 6). Nerve roots that originate from the ventral surface of the placode course anteriorly through the subarachnoid space of the spinal canal and go to the neural foramina (1,3,16,17,23,24).

Hemimyelo(meningo)cele

Hemi–open SD is an extremely rare condition, defined as splitting of the spinal cord (diastematomyelia) in which one hemicord fails to neurulate (failure in primary neurulation process) and is therefore exposed to the environment. There are two types of hemi–open SD: hemimyelomeningocele occurs when there is dorsal expansion of the subarachnoid space that elevates the hemiplacode above the skin surface (Fig 7), and hemimyelocele occurs when the hemiplacode is flush with the skin surface (1,3,17,23).

Embryologically, this dysraphism is related to faulty gastrulation by failed midline notochordal integration, producing the split cord, with a superimposed error of primary neurulation of one hemicord (13,14,21,22).

The neurologic impairment is similar to that seen in patients with diastematomyelia, which includes orthopedic problems such as foot malposition, leg weakness, low back pain, scoliosis, and urinary or fecal incontinence. However, the symptoms are markedly asymmetric, usually worse on the same side of the hemi–open SD (3).

Hemimyelomeningocele will appear as the association at the same level of a diastematomyelia with a myelo(meningo)cele (Fig 7). A fibrous or bony spur dividing the spinal canal may be seen. When it is not seen, the two hemicords lie within a single dural sac, and both could be nonneurulated (failure in primary neurulation process).

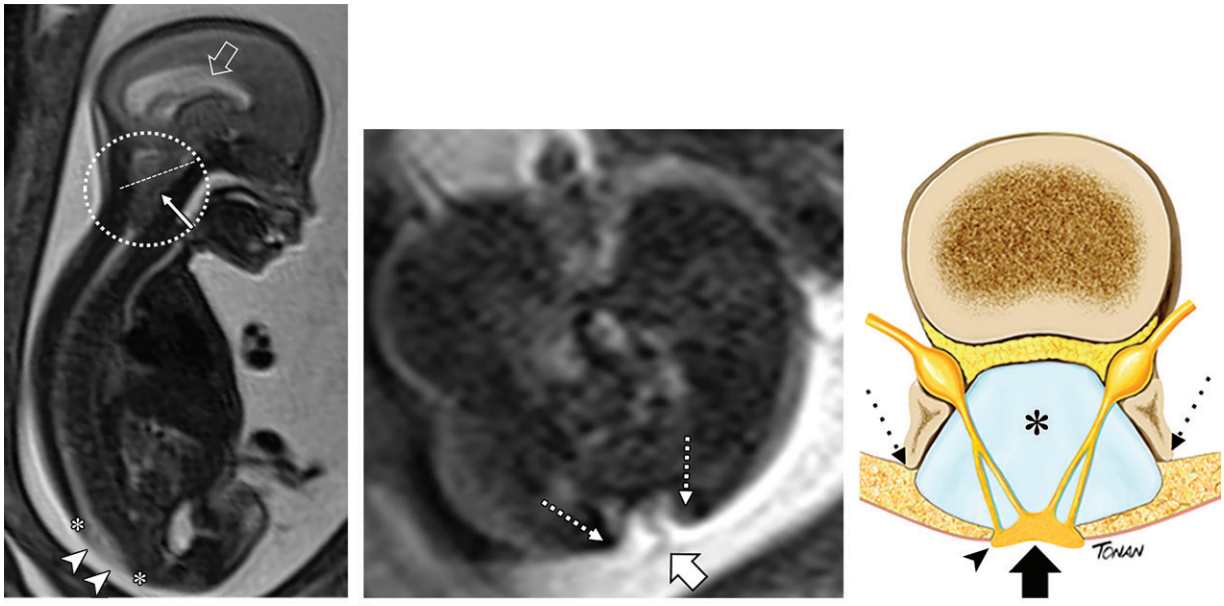

a. b. c.

Figure 6. Myelocele with Chiari II malformation. **(a, b)** Sagittal **(a)** and axial **(b)** single-shot fast spin-echo T2-weighted images of the fetal central nervous system show discontinuity of skin and subcutaneous tissue (∗ in **a**) in the lumbosacral region, with herniation of nervous tissue through the spina bifida (thin arrows in **b**), forming the placode. The placode is flat to the adjacent skin surface (arrowheads in **a**, thick arrow in **b**) and exposed to the amniotic fluid, without expansion of the adjacent subarachnoid space. Chiari II malformation is characterized by a small posterior fossa (dotted white circle in **a**), a slitlike fourth ventricle (thin arrow in **a**), and herniation of the cerebellar tonsils or vermis through the foramen magnum (dotted white line in **a**), determining dilatation of the supratentorial ventricular system (thick arrow in **a**). **(c)** Drawing shows discontinuity of skin and subcutaneous tissue (arrowhead), with the placode (thick arrow) herniated through the spina bifida (thin arrows) and exposed to the environment, on the same plane as the skin surface, without expansion of the underlying subarachnoid space (∗).

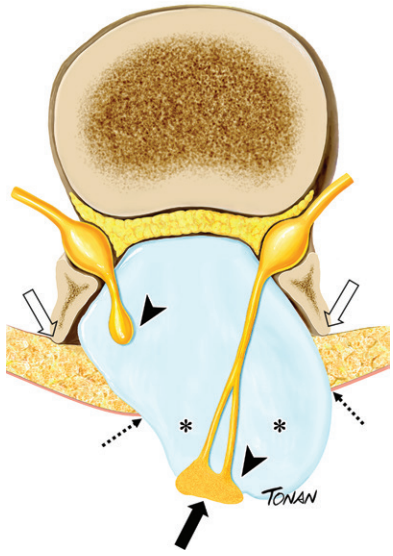

Figure 7. Hemimyelomeningocele. Drawing shows splitting of the spinal cord (arrowheads) at the same level of the open SD, with discontinuity of skin and subcutaneous tissue (dotted arrows) at the side of the hemiplacode that is exposed to the environment (solid arrow). There is a hemimeningocele (∗) protruding posteriorly through the spina bifida (open arrows), raising the placode above the adjacent skin surface.

At MRI, hemimyelomeningocele manifests as splitting of the spinal cord at the same level of the open SD, with discontinuity of skin and subcutaneous tissue at the side of the hemiplacode that is exposed to the environment. It is also important to differentiate imaging features of hemimyelomeningocele and hemimyelocele through the presence or absence, respectively, of the expansion of the subarachnoid space underlying the hemiplacode (1,3,16,17,23,24).

Chiari II Malformation

Chiari II malformation is present in all open SDs and can be considered a continuum of the malformation. The severity of the posterior fossa malformation is variable and can be explained by CSF leak through the SD in the amniotic sac, promoting underdevelopment of the fourth ventricle. The main imaging findings are small posterior fossa, herniation of the brainstem and cerebellar tonsils or vermis through the foramen magnum, dilatation of the supratentorial ventricular system, callosal dysgenesis, and tectal beaking (Figs 5, 6) (1,3,17,23,25).

Closed SDs with Subcutaneous Mass

Lipomas with Dural Defect

Lipomas with dural defect (LDDs) constitute a continuum of abnormalities (lipomyelomeningocele, lipomyelocele, and lipomyeloschisis)

that share a common pathophysiologic process. They differ from each other by the position of the cord-lipoma interface, which is important information for the surgical approach. Together, these anomalies represent 75.9% of all spinal lipomas and 16.4% of all closed SDs (1,17).

The most accepted embryogenic theory involves an error in primary neurulation, with early separation between the cutaneous ectoderm and the neuroectoderm. This allows intervening mesenchymal tissue into the neural tube and formation of a lipomatous mass, preventing successful neurulation.

LDDs are clinically characterized by the presence of a subcutaneous mass of adipose tissue above the intergluteal crease, extending asymmetrically into the buttock. Skin stigmas are found in 50% of patients and may include hypertrichosis, capillary hemangioma, dermal sinus tract (DST), or dimples (1,17). As these stigmas are easily depicted at birth, early surgical approaches are usually instituted, leading to a less pronounced degree of neurologic impairment. It is important to remember that the fat component of LDDs may grow with age, according to the degree of body adipose tissue accumulation.

At MRI, LDD is depicted as an intradural lipomatous mass attached to the spinal cord, configuring the cord-lipoma complex. It is important to report the position and dimensions of the cord-lipoma complex, as well as its relationship with other structures. SD can rarely coexist and be associated with split cord malformations (diastematomyelia) (18).

Lipomyelomeningocele.—Lipomyelomeningocele is characterized by the combination of a subcutaneous lipoma with a posterior meningocele (3). MRI shows enlargement of the spinal canal with expansion of the subarachnoid space. The low-lying spinal cord crosses into the meningocele and attaches to a subcutaneous lipoma. The cord-lipoma interface is located outside the vertebral canal and usually occurs off midline, with traction of the placode toward the lipoma on one side and meningeal herniation on the other (Fig 8).

The neural roots exhibit an aberrant course. Those that emerge from the side where the meningocele prevails tend to be long and more susceptible to trauma, while those that are close to the placode tend to be short and promote tethering of the spinal cord (1,17).

Lipomyelocele and Lipomyeloschisis.—These subtypes of closed SD share similar imaging findings and are characterized by a posterior neural arch defect (spina bifida), through which a lipomatous subcutaneous mass penetrates the spinal canal and attaches to the tethered cord (3). The spinal canal can be expanded depending on the size of the lipoma, but there is no evidence of meningeal herniation or expansion of the subarachnoid space. The distinguishing factor between these two conditions is the position of the cord-lipoma interface: at the level of the neural arches (lipomyelocele) (Fig 9) or within the spinal canal (lipomyeloschisis) (Fig E1).

Although lipomyeloschisis is more common than lipomyelocele, these terms are often used interchangeably, since the two conditions are often not clearly separable from one another. This is a result of cord stretching and variable length of the cord-lipoma interface, which may extend over several vertebral levels (1,3,17).

Meningocele

Meningocele is a CSF hernia delineated by a dural and arachnoid lining through a posterior spina bifida; meningoceles do not contain neural tissue, which explains the usually mild neurologic condition. These cystic formations are covered by soft tissue and skin and may manifest with alterations, such as cutaneous dystrophy, hemangioma, or tail-like protrusion (3,26). As the meningeal lining is formed late in the embryologic process, posterior congenital meningoceles probably occur at week 7 of gestation (27). The exact embryogenic mechanism is uncertain, but it is believed that there is failure of separation between the meninx primitiva and cutaneous ectoderm, which herniate through the posterior spina bifida, promoted by constant CSF pulsation (3). Meningoceles correspond to approximately 10% of myelomeningoceles (28), representing about 2.4% of all closed SDs (1,17).

At MRI, meningocele appears as an extraspinal hernia of the meninges through a spina bifida and is filled only with CSF (Fig 10). Rarely, redundant nerve roots may be depicted within the sac on high-resolution T2-weighted images, or a hypertrophic filum terminale may course within the meningocele. The spinal cord is structurally normal (1,3,17).

Myelocystocele

Myelocystocele is defined as herniation of a hydrosyringomyelic cavity through the spina bifida into a meningocele. Myelocystocele can occur at any level of the spine. It is classified as terminal when located in the lumbosacral region or as nonterminal when it occurs in the cervical or thoracic segment (3,29,30).

The two subtypes differ in epidemiologic, embryologic, and clinical-radiologic aspects. Terminal myelocystocele is more common, representing approximately 5% of all closed SDs with a higher

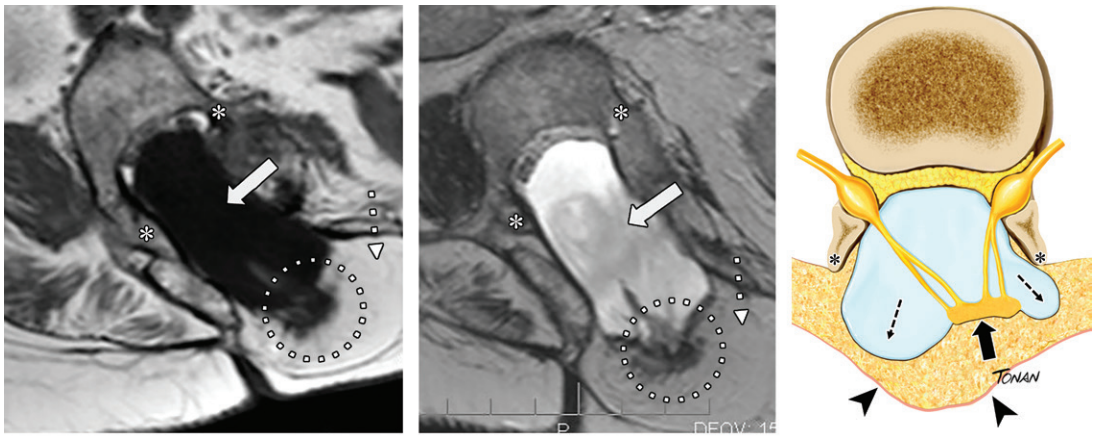

a. b. c.

Figure 8. Lipomyelomeningocele. **(a, b)** Axial T1-weighted **(a)** and T2-weighted **(b)** images of the lumbar spine show the placode (dotted white circle) attached to a lipoma (dotted arrow), forming the cord-lipoma interface, which is located outside the spinal canal owing to expansion of the underlying subarachnoid space (solid arrow), which protrudes through the spina bifida (*). **(c)** Drawing shows the skin and subcutaneous tissue (arrowheads) covering the placode (solid arrow), which is anchored to adipose tissue outside the vertebral canal and off midline owing to asymmetric expansion of the underlying subarachnoid space (dashed arrows), both herniating through the spina bifida (*).

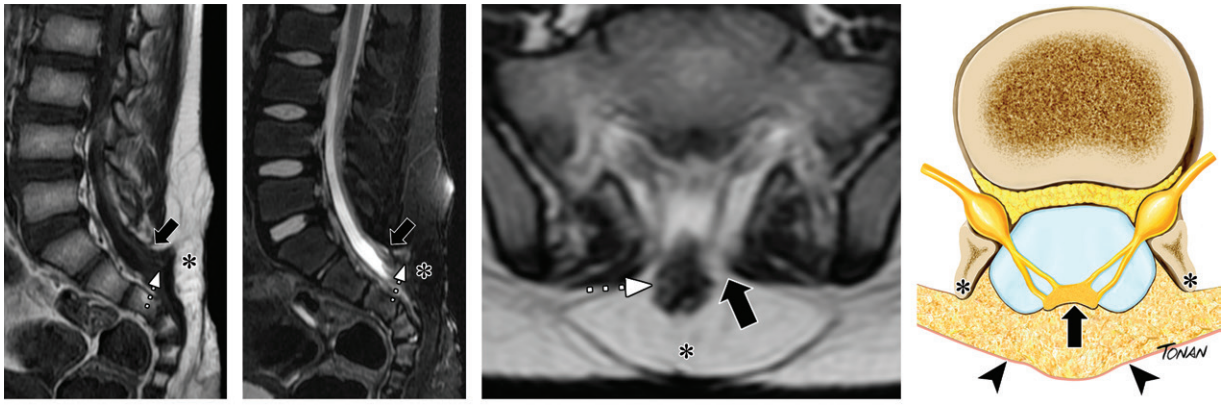

a. b. c. d.

Figure 9. Lipomyelocele. **(a, b)** Sagittal T1-weighted **(a)**, sagittal fat-saturated T2-weighted **(b)**, and axial T2-weighted **(c)** images of the lumbosacral spine show a lipomatous mass (solid arrow) insinuating into the spinal canal and communicating with the subcutaneous region posteriorly (*). The placode-lipoma interface (dotted arrow) is located at the level of the neural arches, without expansion of the subarachnoid space. **(d)** Drawing shows a skin-covered posterior arch defect (*) characterized by a subcutaneous lipomatous mass (arrowheads), which penetrates the spinal canal through a posterior spina bifida and attaches to the placode (arrow). The cord-lipoma interface lies at the level of the neural arches, without expansion of the subarachnoid space.

prevalence in females (31). Embryologically, terminal myelocystocele is generally seen as a defect in secondary neurulation. The cavity of the persistent secondary neural tube inflates, promoting rupture of the surrounding mesenchymal tissue.

Nonterminal myelocystocele occurs during primary neurulation owing to incomplete fusion of the neural tube, with failure of separation of the ectoderm from the neuroectoderm. Formation of the lining of the adjacent skin configures a closed spinal malformation. Because of the failure to separate of the two embryonic leaflets—ectoderm and neuroectoderm—there is formation of a fibroneurovascular filament, which extends from the posterior wall of the spinal cord through the meningocele and the opening of the dura and adheres to abnormal skin. Continuous CSF pulsation inflates the posterior wall of the medullary ependymal canal through the spina bifida and meningocele, forming a hydrosyringomyelic cavity (3).

MRI of terminal myelocystocele shows a low spinal cord ending in a large hydrosyringomyelic cavity that herniates through the spina bifida into a meningocele, anchoring in its posterior wall. The terminal hydrosyringomyelic cavity is a continuation of the ependymal canal, while the meningocele is an expansion and herniation of the subarachnoid space. Thus, the CSF of the syringomyelia does not usually communicate with the CSF of the meningocele (Fig 11). The OEIS complex (*o*mphalocele, *e*xstrophy of the cloaca,

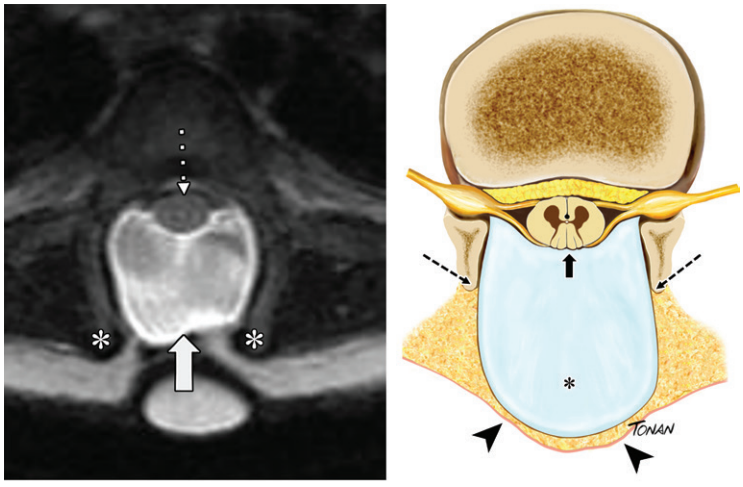

Figure 10. Meningocele. **(a)** Axial T2-weighted image of the thoracic spine shows a cerebrospinal fluid (CSF)–filled meningeal hernia (solid arrow) through a posterior spina bifida (*). The thoracic spinal cord is normal (dotted arrow), and there are no neural elements inside the outpouching. **(b)** Drawing shows a CSF-filled meningeal hernia (*) through a spina bifida (dashed arrows), covered by skin and subcutaneous tissue (arrowheads) with a normal spinal cord (solid arrow).

*i*mperforate anus, *s*pinal dysraphism) is usually associated with terminal myelocystocele (16).

At MRI, nonterminal myelocystocele shows the posterior wall of the hydrosyringomyelic cavity herniating through the bifid spine into the meningocele, with the anterior wall of the spinal cord withheld in the vertebral canal (16,32).

Closed SDs without Subcutaneous Mass

Simple Dysraphic States

Intradural Lipoma.—Intradural lipoma is a benign elongated lesion composed of adipose cells contained within the dural sac, unlike lipoma with dural defect (LDD) (33,34). It represents about 24% of all spinal lipomas and is frequently located in the lumbosacral spine, but may be found at any level as a focal mass or showing multifocality and diffuse distribution (1,17,35,36). As with LDD, the embryologic origin involves an error in primary neurulation, with early separation between the cutaneous ectoderm and neuroectoderm, allowing insinuation of intervening mesenchymal tissue into the neural tube and formation of a lipomatous mass and preventing successful neurulation (1,3,17).

The clinical picture depends primarily on the size and location of the lipoma. If there is mass effect, cord compression syndrome will prevail in cervical and dorsal intradural lipomas. As with LDD, intradural lipoma can increase in size during child growth (3,31).

At MRI, intradural lipoma is depicted as a subpial lipomatous lesion lying between the folds of the placode. Large lipomas can displace the spinal cord and appear off midline (Fig E2). Rarely, it is seen as an intramedullary lesion or even as intramedullary lipomatosis (1,3,17,31).

Lipoma of Filum Terminale.—Filum terminale lipoma (filar lipoma) is due to an abnormality of secondary neurulation, in which impaired canalization of the tail bud and persistence of cells capable of maturing into adipocytes are likely to be involved. This process occurs after disjunction of the cutaneous and neural ectoderm. This lesion is covered by skin and lacks cutaneous stigmas (20).

The exact prevalence of filar lipoma in the general population is unknown because most patients are asymptomatic (95%). Cools et al (37) reported an estimated prevalence of about 0.2%–4% in the adult population at MRI.

At MRI, filar lipoma appears as a small lipomatous lesion in the filum terminale region with no communication with the medullary cone (Fig E3). It can be associated with other conditions, especially type II caudal agenesis syndrome or tethered cord syndrome (4,37).

Although filar lipoma and fatty filum terminale (FFT) have similar embryopathology, it is important to differentiate them at imaging. The latter is defined as lipomatous infiltration of the filum terminale with a maximum thickness of 2.0 mm. FFT is not clinically relevant (37).

Persistence of Terminal Ventricle.—Historically known as the "fifth ventricle," persistent terminal ventricle consists of a small ependyma-lined cavity centrally located within the conus medullaris (27). An error during secondary neurulation leads to incomplete regression of the terminal ventricle. A critical point is that continuity with the central canal of the rostral spinal cord is preserved. This differs from myelocystocele, in which this connection is not preserved, leading to a more severe condition (20).

Most cases of persistent terminal ventricle are asymptomatic. According to the size of the cystic

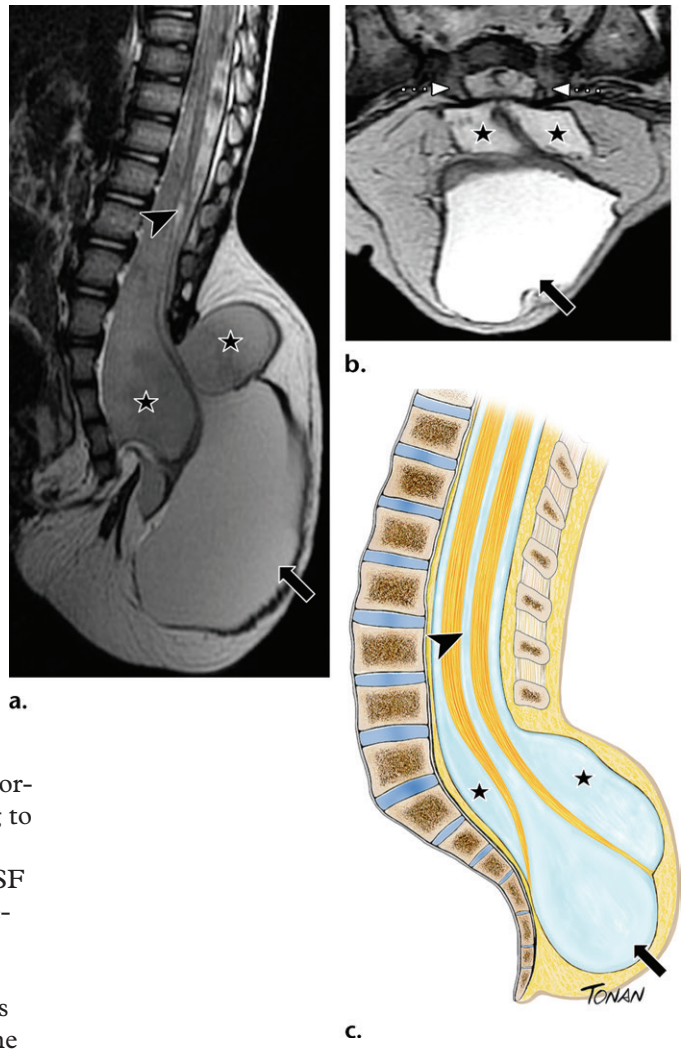

Figure 11. Myelocystocele. Sagittal **(a)** and axial **(b)** T2-weighted images and drawing **(c)** show a low spinal cord ending in a large hydrosyringomyelic cavity (solid arrow), which herniates through the spina bifida (dotted arrows in **b**) into a meningocele (★) and anchors in its posterior wall. The terminal hydrosyringomyelic cavity is a continuation of the ependymal canal (arrowhead in **a** and **c**) that is dilated. Note that the cerebrospinal fluid (CSF) of the syringomyelia does not communicate with the CSF of the meningocele. (Fig 11a and 11b courtesy of Ricardo Mendes Rogerio, MD, Santa Casa de Misericórdia do Estado do Pará, Belém-Pa, Brazil.)

dilatation, some patients may have bladder disorders, low back pain, or sciatica, possibly owing to thinning of the conus medullaris (38).

At MRI, the cystic cavity is isointense to CSF with all sequences and does not show enhancement (Fig E4). In most cases, the size of the cystic cavity remains stable at follow-up but may rarely increase owing to valve mechanisms (17). In 1995, Coleman et al (39) measured the dimensions of the terminal ventricle with MRI in 11 children. They found an average size of 22 mm in length (range, 15–30 mm), 4.1 mm in anteroposterior diameter (range, 1.5–6 mm), and 4.2 mm in transverse diameter (range, 1.5–6 mm).

Complex Dysraphic States

Dermal Sinus Tract.—Dermal sinus tract (DST) or dorsal dermal sinus is defined as a midline fistula lined by epithelium that connects the skin surface with the central nervous system or its meningeal membranes. The lumbosacral region is the most common site of involvement, with DST being rare in the occipital, cervical, and thoracic regions. Its prevalence is estimated at one in 2500 living births, and there is no sex predilection (29).

Embryologically, DST is the result of focal failure in disjunction of the neuroectoderm from the ectoderm during primary neurulation. The lumbosacral region is the last place where fusion of the neural folds occurs, with subsequent closure of the neural tube. Therefore, there is a greater chance of failure of separation between the neuroectoderm and the cutaneous ectoderm, increasing the prevalence of DST at that location.

At physical examination, an ostium is observed in the midline of the skin surface, most commonly at the S2 level. It can occur in any vertebral segment and may be associated with capillary angioma, hairy nevus, or hyperpigmented patch. If associated with an inclusion cyst, then clinical symptoms of infection or even compression of neural structures may occur. DST can connect the skin surface to any level of the subpial space, causing several complications, such as meningitis, abscess, and CSF leak. Chemical meningitis can occur when a dermoid cyst associated with the dermal sinus ruptures in the subarachnoid space.

MRI demonstrates a thin band, coursing through the subcutaneous tissue with an oblique and descending trajectory. Moreover, it extends from the skin surface to the vertebral canal and is usually detected in the sagittal and axial planes (Fig E5). Heavily T2-weighted sequences (eg, constructive interference in steady state [CISS]

or fast imaging employing steady-state acquisition [FIESTA]) should be included in the protocol owing to their high sensitivity in depicting the DST. MRI can also depict associated malformations, such as ectodermal inclusion cysts.

Therefore, it is important to include diffusion-weighted imaging (DWI) sequences, which allows differentiation of dermoid cysts from epidermoid cysts. Epidermoid cysts often exhibit restricted diffusion. In case of associated infectious complications, in addition to DWI, contrast-enhanced fat-saturated T1-weighted imaging may reveal abnormal gadolinium enhancement of the dura, cauda equina roots, and pial surface of the conus medullaris or even show characteristic peripheral enhancement of the abscess wall (Fig E5).

Diastematomyelia.—Diastematomyelia, a type of split-cord malformation (3), is defined by division of the spinal cord into two hemicords, each covered by its own layer of pia mater and having its own central canal. Each hemicord gives rise to a pair of horns, one ventral and one dorsal (where the corresponding nerve roots originate). This malformation accounts for approximately 3.8% of all closed SDs. It is divided into type I and type II, with females affected more commonly than males. It is more common in the lumbar region (>80% of cases) and can be associated with vertebral anomalies and hydromyelia, especially in type I (17).

During gastrulation, midline integration occurs in which the two paired notochordal anlagen fuse in the midline to form a single notochordal process. If these notochordal precursors fail to integrate, then they remain separate and develop independently over a variable segment. The intervening space will be occupied by totipotential primitive streak cells (19).

Differentiation between the two types of diastematomyelia depends on development of primitive streak tissue. In type I, the intervening primitive streak develops into bone or cartilage, creating a septum (radiologic mark) that separates the dural sac in two. In type II, the primitive streak is reabsorbed or forms a fibrous septum, with a single dural sac involving both hemicords.

Clinical symptoms are variable and usually related to orthopedic problems, such as foot malposition, leg weakness, low back pain, scoliosis, and urinary or fecal incontinence. Cutaneous birthmarks—such as hairy tuft, nevus, lipoma, dimple, or hemangioma—in the lumbar region can be a distinctive finding at physical examination (1,17,27).

In type I diastematomyelia, both hemicords have their individual dural sacs and are separated by an osteocartilaginous or bony septum. Osteocartilaginous separation is most characteristic. The septum is extradural and usually extends from the vertebral body to the posterior elements. Vertebral abnormalities are often present (eg, bifid lamina, hemivertebra, or bifid vertebra) (Fig 12).

Type II diastematomyelia is characterized by a single dural sac containing both hemicords, without an osteocartilaginous or bony septum. Vertebral anomalies are usually milder than in type I (eg, bifid spinous process). Heavily T2-weighted sequences (eg, CISS or FIESTA) can be useful for depicting the nerve root course and the relationship between the hemicords and the septum (3) (Fig 13).

Caudal Regression Syndrome.—Caudal regression syndrome (CRS), caudal regression sequence, or sacral agenesis (40) comprises a range of abnormalities in the lower half of the body, including lumbosacral agenesis, along with variable malformations in the lower limbs and genitourinary and gastrointestinal systems and pulmonary hypoplasia (Table 2).

CRS is estimated to occur in 1.3 per 10 000 newborns. It is a cardinal feature of diabetic embryopathy, with an estimated risk 170–400 times higher in infants born to mothers with pregestational diabetes mellitus than in the general population (41). Other proposed contributing factors include genetic predisposition (*HLXB9* gene mutation), vascular anomalies altering blood flow, and drugs (eg, minoxidil, trimethoprim sulfamethoxazole, tocilizumab). With rare exceptions, the fetal karyotype is normal (40).

CRS results from abnormal development of the tail bud during the interface between primary and secondary neurulation before the 4th week of gestation. This abnormal development of the tail bud impairs the normal migration of neurons and the paraxial and lateral mesoderm cells, leading to errors in development of the skeletal, gastrointestinal, and genitourinary systems (41).

The spectrum of neurologic findings varies from mild and isolated foot deformity to complete paralysis of both lower extremities, with motor deficits being more severe than the sensory loss. Other findings include flattened buttocks, narrow hips, short intergluteal cleft, neurogenic bladder, and sphincter dysfunction.

There are two types of CRS, which can be classified according to the degree of vertebral dysgenesis and the shape and location of the medullary cone. In type I, there is a major degree of vertebral abnormalities, and MRI reveals vertebral dysgenesis that may extend from the low thoracic region to the coccygeal region.

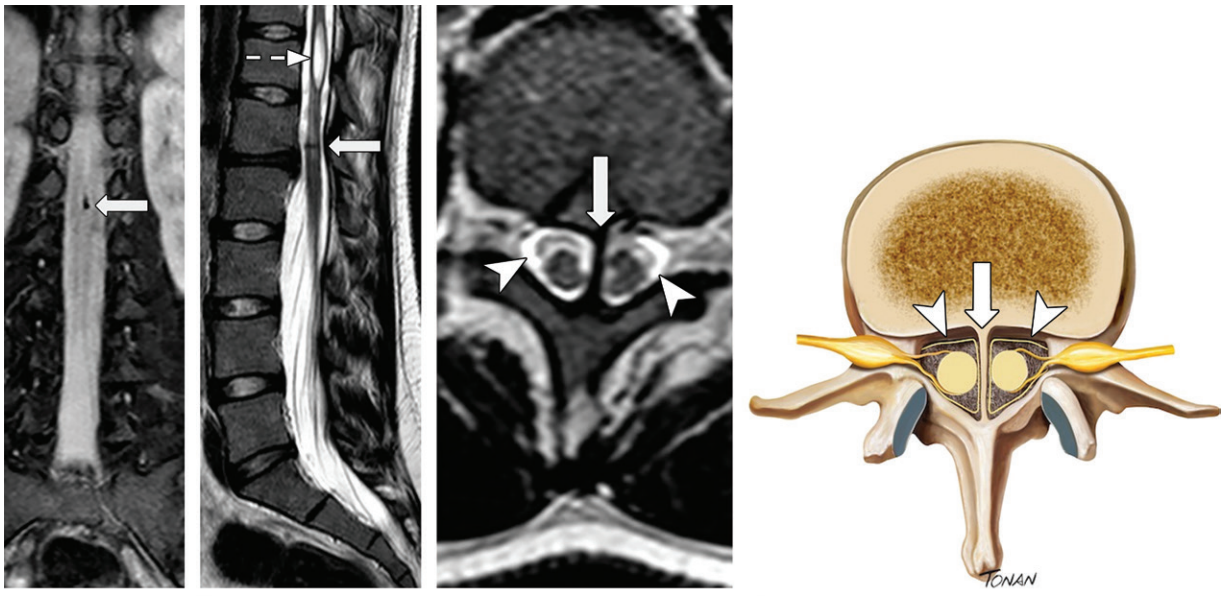

Figure 12. Type I diastematomyelia. Coronal **(a)**, sagittal **(b)**, and axial **(c)** T2-weighted images of the lumbosacral spine and drawing **(d)** show two hemicords, each surrounded by its own dural sac (arrowheads in **c**, **d**), which are separated by an osteocartilaginous or bony spur (solid arrow). There is a hydrosyringomyelic cavity (dashed arrow in **b**) cranial to the diastematomyelia.

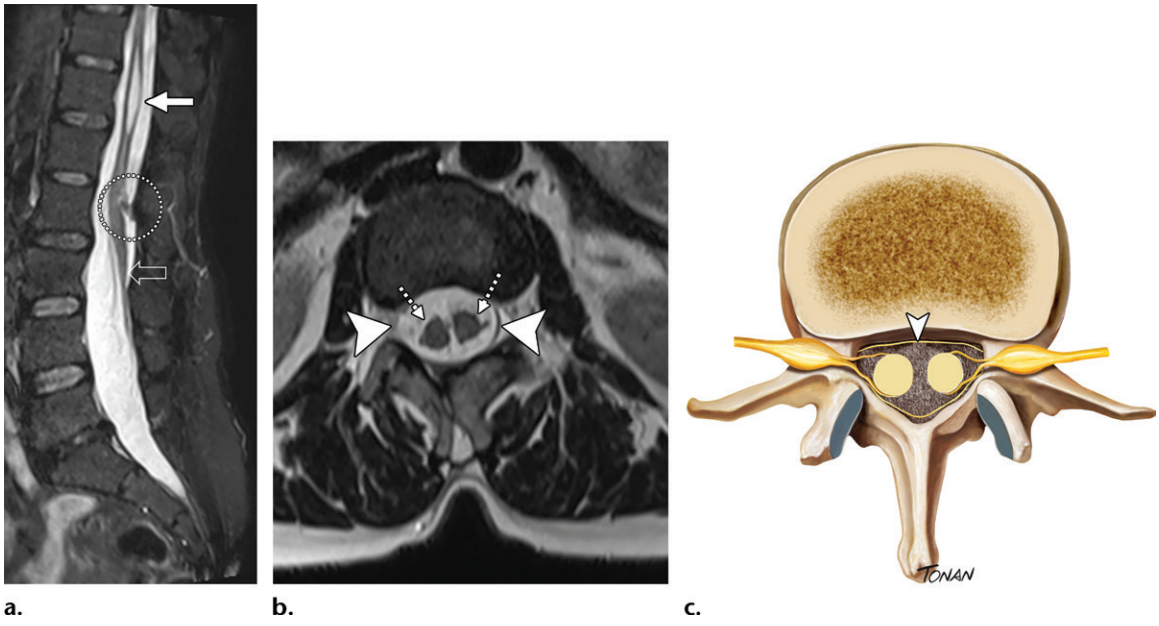

Figure 13. Type II diastematomyelia associated with tethered cord, intradural lipoma, and syringomyelia. Sagittal fat-saturated T2-weighted **(a)** and axial T2-weighted **(b)** images of the lumbosacral spine and drawing **(c)** show a spinal cord split into two hemicords (arrows in **b**), both surrounded by the same and only dural sac (arrowheads in **b**, **c**), with no identified osteocartilaginous or bony spur. The end of the spinal cord is low and attached to the thickened filum terminale (open arrow in **a**). Note the associated intradural lipoma (dotted white circle in **a**) and syringomyelia (solid arrow in **a**).

The conus medullaris is often high and has an abrupt terminus, usually associated with parallelism ("double-bundle shape") of the roots of the cauda equina (Fig 14). Type I can result from abnormalities at the end of primary neurulation and interruption of secondary neurulation.

Imaging of type II CRS usually demonstrates less severe vertebral dysgenesis (eg, segmental agenesis of the sacral vertebrae or the entire coccyx), and the caudal end of the spinal cord is almost always tethered to an intraspinal mass (eg, lipomyelocystocele, spinal lipoma, anterior sacral meningocele). Absence of the tip of the medullary cone can also be found (Fig 15). Type II is related to abnormalities of secondary neurulation.

Limited Dorsal Myeloschisis.—Limited dorsal myeloschisis (LDM) is a unique form of SD

Table 2: Associated Anomalies in Caudal Regression Syndrome

System	Anomalies
Musculoskeletal	Knee and hip flexion contractures, lower limb deformities, kyphoscoliosis, fusion or absence of ribs, polydactyly, syndactyly, hypoplastic gluteal muscles, shallow intergluteal cleft
Gastrointestinal	Anorectal anomalies, abdominal wall defects, duodenal or colonic atresia, malrotation, hernia, fistula
Genitourinary	Renal agenesis or dysplasia, horseshoe kidney, hydronephrosis, ectopic ureter, vesicoureteral reflux, ureteral atresia, absent bladder, ambiguous genitalia
Others	Neural tube defects, facial clefts, congenital heart disease, pulmonary hypoplasia, VACTERL* syndrome, Currarino triad†

*VACTERL = *v*ertebral, *a*norectal, *c*ardiac, *t*racheal, *e*sophageal, *r*enal, and *l*imb anomalies.
†Anorectal malformation, sacrococcygeal osseous defect, and presacral mass.

that can be promptly diagnosed with MRI and is characterized by two main features: a focal "closed" midline skin defect and a fibroneural tract connecting the underlying spinal cord to the skin (Fig E6) (42–45). It is an uncommon disease, with less than 200 cases reported in the literature. LDM is divided into two main groups: nonsaccular and saccular, with the former being the most common. It can be found in all of the spinal neuraxis, with the lumbar segment being the most commonly affected, and is usually accompanied by skin lesions (42).

Pang et al (45) hypothesized that LDM is related to incomplete disjunction between the neural and cutaneous ectoderm during primary neurulation, given that the fibroneural stalk was attached to the cord above the S1-S2 level.

Neurologic deficits are variable and usually related to the location of the LDM (42–44), with the cervical spine being the most frequent segment associated with neurologic symptoms.

In the nonsaccular form, MRI often demonstrates a stalk that communicates with the dorsal surface of the spinal cord, with an underlying malformation of the posterior vertebral elements that can be associated with subcutaneous or skin lesions. The spinal cord has a characteristic trapezoid shape in the axial plane near the level of the stalk-cord union (43). Detailed description of the saccular form is beyond the scope of this article and can be found elsewhere (44,45).

Segmental Spinal Dysgenesis.—Segmental spinal dysgenesis (SSD) is a rare congenital abnormality characterized by localized agenesis or dysgenesis of the spine and spinal cord. It can affect any segment of the spine but is more frequent in the lower levels, with higher prevalence in the thoracolumbar and upper lumbar spine (46).

It is believed that SSD results from deregulated apoptotic events during gastrulation in which wrongly specified cells are eliminated owing to incorrect positional imprinting during chordal-mesodermal cell migration through the primitive pit, leading to embryonic segmental malformation (1,46,47).

Clinically, patients present with a kyphotic deformity (sharply angled), hyperreflexia of the lower extremities, and lower limb abnormalities (flexion-abduction of the hip joints, flexion of the knees, and equinovarus feet, which in the most severe forms result in a sitting position described as "Buddha-like") (46). Cutaneous stigmas may be seen on the overlying skin. Associated visceral organ anomalies can be present and may include the urinary, anorectal, and cardiovascular systems (48).

MRI demonstrates involvement of one segment of the spine, with normal vertebrae below and above the anomaly and a characteristic kyphotic deformity. Agenesis or hypogenesis of the involved vertebral body may be associated with other vertebral abnormalities, like aplastic or hypoplastic vertebra, hemivertebra, and butterfly vertebra (46,48). The spinal cord at the level of the deformity is thinned or completely absent, with a normal spinal cord above the segment. Usually, a bulky and low-lying cord can be found below the abnormality.

The main differential diagnosis for SSD includes CRS. Despite sharing a similar embryologic basis, CRS represents a different condition (46).

Multiple SDs.—Multiple SD forms or multiple-site neural tube defects are rare, accounting for less than 1% of neural tube defects (49,50), and are defined by the presence of more than one malformation with normal neural tissue between them. They must be differentiated from complex spinal defects, which are characterized by many different defects in a contiguous distribution (49). The exact origin of these combined malformations (Fig E7) is unknown. There are many theories that try to explain them, with the most

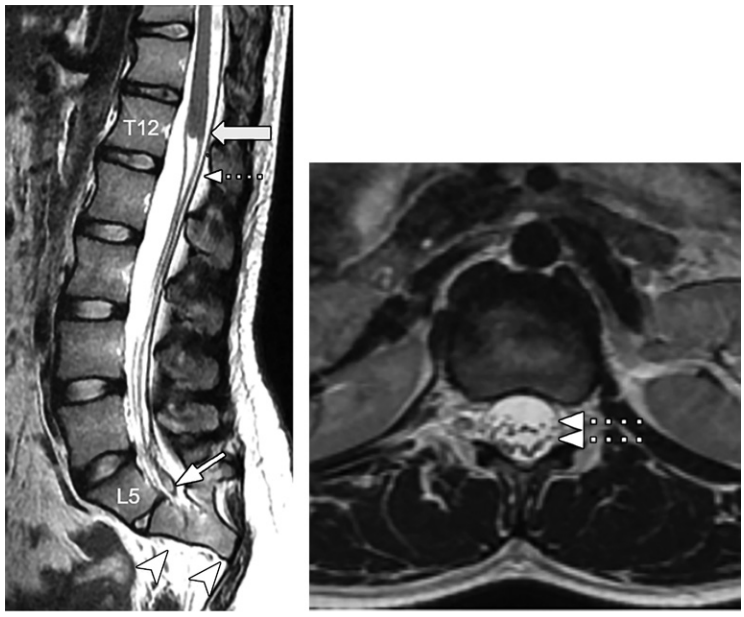

Figure 14. Type I caudal regression syndrome. Sagittal **(a)** and axial **(b)** T2-weighted images of the lumbosacral spine show partial agenesis of the sacrococcygeal spine (arrowheads in **a**) and abrupt termination of the conus medullaris at the T12 level (thick solid arrow in **a**), which has a wedge-shaped appearance. The nerve roots have an abnormal path, configuring a "double-bundle shape" (dotted arrows). The dural sac has high termination, with closure just after the end of L5 (thin solid arrow in **a**).

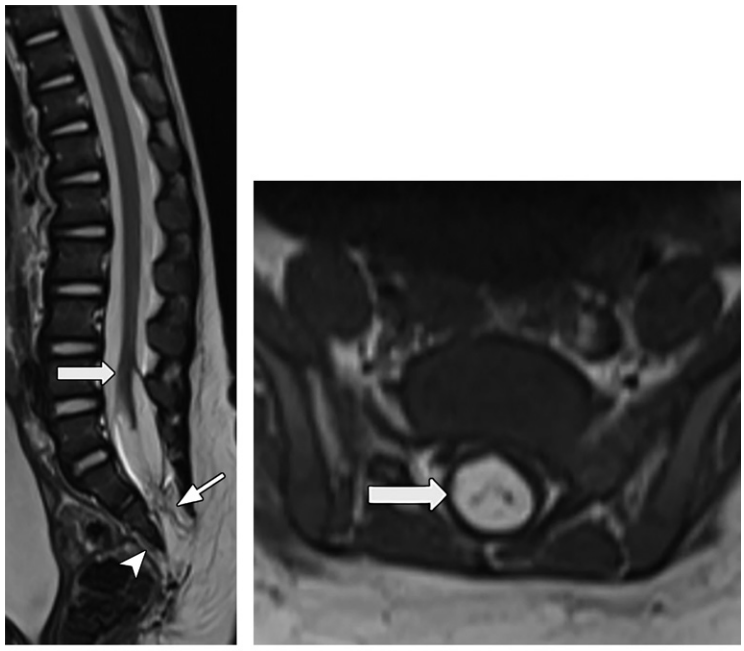

Figure 15. Type II caudal regression syndrome and lipomyeloschisis. Sagittal **(a)** and axial **(b)** T2-weighted images of the lumbosacral spine show partial agenesis of the sacrococcygeal spine (arrowhead in **a**), with some upper sacral vertebral segments still visible. The spinal cord is tethered at the L4-L5 level and anchored to an intradural lipoma (thick arrow), which communicates with the fat from the posterior sacral subcutaneous tissue (thin arrow in **a**).

accepted called the multisite closure theory (49), which is beyond the scope of this article.

Conclusion

Congenital malformations of the spinal cord represent a heterogeneous group of abnormalities that usually occur owing to derangements in the steps of the complex cascade of spinal embryology. As discussed earlier, they are divided into two main groups: open SDs, which represent a medical emergency owing to direct environmental exposure of neural tissue, and closed SDs, in which the anomalies show skin coverage. SDs represent an important cause of childhood morbidity owing to not only neurologic impairment but also associated malformations, as in the respiratory and gastrointestinal tracts, leading to profound economic and psychosocial impact. Neuroimaging plays a pivotal role in diagnosis and presurgical evaluation of SDs. Therefore, knowledge of spinal cord embryology and the main imaging findings of these malformations is essential for the radiologist.

Acknowledgments.—The authors thank G.D.G. and T.d.A.L.F. for the exceptional technical and scientific support, André Maia Ribeiro for collaborating with the creative process of the

manuscript, and Rodrigo Tonan for enriching the content of the manuscript through impeccable medical illustrations.

References

1. Schwartz EC, Barkovich AJ. Congenital Anomalies of the Spine. In: Zinner S, Pecarich L, eds. Pediatric neuroimaging. 6th ed. Philadelphia, Pa: Wolters Kluwer, 2018; 1311–1377.
2. Neural Tube Defects, Susceptibility to; NTD. OMIM: Online Mendelian Inheritance in Man. https://www.omim.org/entry/182940. Published June 2, 1986. Updated August 11, 2016. Accessed March 28, 2020.
3. Rossi A. Imaging in Spine and Spinal Cord Developmental Malformations. In: Barkhof F, Jäger HR, Thurnher MM, Rovira A, eds. Clinical Neuroradiology: The ESNR Textbook. Cham, Switzerland: Springer, 2018; 1609–1640.
4. Asma B, Dib O, Chahinez H, et al. Imaging findings in spinal dysraphisms. EPoster C-1516, 2017 European Congress of Radiology. https://doi.org/10.1594/ecr2017/C-1516. Published 2017. Accessed April 2, 2020.
5. Passias PG, Poorman GW, Jalai CM, et al. Incidence of Congenital Spinal Abnormalities Among Pediatric Patients and Their Association With Scoliosis and Systemic Anomalies. J Pediatr Orthop 2019;39(8):e608–e613.
6. Aoulad Fares D, Schalekamp-Timmermans S, Nawrot TS, Steegers-Theunissen RPM. Preconception telomere length as a novel maternal biomarker to assess the risk of spina bifida in the offspring. Birth Defects Res 2020;112(9):645–651.
7. Lei YP, Zhang T, Li H, Wu BL, Jin L, Wang HY. VANGL2 mutations in human cranial neural-tube defects. N Engl J Med 2010;362(23):2232–2235.
8. Copp AJ, Stanier P, Greene NDE. Genetic Basis of Neural Tube Defects. In: Di Rocco C, Pang D, Rutka J, eds. Textbook of Pediatric Neurosurgery. Cham, Switzerland: Springer, 2017; 1–28.
9. Schorah C. Dick Smithells, folic acid, and the prevention of neural tube defects. Birth Defects Res A Clin Mol Teratol 2009;85(4):254–259.
10. van Gool JD, Hirche H, Lax H, De Schaepdrijver L. Folic acid and primary prevention of neural tube defects: a review. Reprod Toxicol 2018;80:73–84.
11. Mills JL, McPartlin JM, Kirke PN, et al. Homocysteine metabolism in pregnancies complicated by neural-tube defects. Lancet 1995;345(8943):149–151.
12. Zohn IE, Sarkar AA. The visceral yolk sac endoderm provides for absorption of nutrients to the embryo during neurulation. Birth Defects Res A Clin Mol Teratol 2010;88(8):593–600.
13. Blount JP, George TM, Koueik J, Iskandar BJ. Concepts in the neurosurgical care of patients with spinal neural tube defects: an embryologic approach. Birth Defects Res 2019;111(19):1564–1576.
14. ten Donkelaar HJ, Yamada S, Shiota K, van der Vliet T. Overview of the Development of the Human Brain and Spinal Cord. In: ten Donkelaar HJ, Lammens M, Hori A, eds. Clinical Neuroembryology: Development and Developmental Disorders of the Human Central Nervous System. 2nd ed. Cham, Switzerland: Springer, 2014; 9–15.
15. Pomeroy S, Yuskaitis CJ. Development of the Nervous System. In: Polin RA, Abman SH, Rowitch D, Benitz WE, eds. Fetal and Neonatal Physiology E-Book. 5th ed. Philadelphia, Pa: Elsevier, 2017; 1294–1313.
16. Rossi A, Biancheri R, Cama A, Piatelli G, Ravegnani M, Tortori-Donati P. Imaging in spine and spinal cord malformations. Eur J Radiol 2004;50(2):177–200.
17. Tortori-Donati P. Congenital Malformations of the Spine and Spinal Cord. In: Tortori-Donati P, Rossi A, eds. Pediatric Neuroradiology. Cham, Switzerland: Springer, 2005; 1551–1608.
18. Reghunath A, Ghasi RG, Aggarwal A. Unveiling the tale of the tail: an illustration of spinal dysraphisms. Neurosurg Rev 2019. 10.1007/s10143-019-01215-z. Published online December 7, 2019.
19. Dias MS, Walker ML. The embryogenesis of complex dysraphic malformations: a disorder of gastrulation? Pediatr Neurosurg 1992;18(5-6):229–253.
20. Kumar J, Afsal M, Garg A. Imaging spectrum of spinal dysraphism on magnetic resonance: a pictorial review. World J Radiol 2017;9(4):178–190.
21. Tortori-Donati P, Rossi A, Cama A. Spinal dysraphism: a review of neuroradiological features with embryological correlations and proposal for a new classification. Neuroradiology 2000;42(7):471–491.
22. Dias MS, Partington M. Embryology of myelomeningocele and anencephaly. Neurosurg Focus 2004;16(2):E1.
23. Kaufman BA. Neural tube defects. Pediatr Clin North Am 2004;51(2):389–419.
24. Parmar H, Patkar D, Shah J, Maheshwari M. Diastematomyelia with terminal lipomyelocystocele arising from one hemicord: case report. Clin Imaging 2003;27(1):41–43.
25. Cama A, Tortori-Donati P, Piatelli GL, Fondelli MP, Andreussi L. Chiari complex in children: neuroradiological diagnosis, neurosurgical treatment and proposal of a new classification (312 cases). Eur J Pediatr Surg 1995;5(suppl 1):35–38.
26. Rufener SL, Ibrahim M, Raybaud CA, Parmar HA. Congenital spine and spinal cord malformations: pictorial review. AJR Am J Roentgenol 2010;194(3 suppl):S26–S37.
27. O'Rahilly R, Müller F. Developmental stages in human embryos: revised and new measurements. Cells Tissues Organs 2010;192(2):73–84.
28. Dias M, Partington M; Section on Neurologic Surgery. Congenital Brain and Spinal Cord Malformations and Their Associated Cutaneous Markers. Pediatrics 2015;136(4):e1105–e1119.
29. Muthukumar N. Terminal and nonterminal myelocystoceles. J Neurosurg 2007;107(2 suppl):87–97.
30. Awad T. Terminal Myelocystocele: A Rare Variant of Spinal Dysraphism—Case Series and Review of the Literature. Egypt Spine J 2016;17(1):28–33.
31. Byrd SE, Harvey C, McLone DG, Darling CF. Imaging of terminal myelocystoceles. J Natl Med Assoc 1996;88(8):510–516.
32. Rossi A, Piatelli G, Gandolfo C, et al. Spectrum of nonterminal myelocystoceles. Neurosurgery 2006;58(3):509–515; discussion 509–515.
33. Shen SH, Lirng JF, Chang FC, et al. Magnetic resonance imaging appearance of intradural spinal lipoma. Zhonghua Yi Xue Za Zhi (Taipei) 2001;64(6):364–368.
34. Pasalic I, Brgic K, Nemir J, Kolenc D, Njiric N, Mrak G. Intramedullary Spinal Cord Lipoma Mimicking a Late Subacute Hematoma. Asian J Neurosurg 2018;13(4):1282–1284.
35. Patwardhan V, Patanakar T, Patkar D, Armao D, Mukherji SK. MR imaging findings of intramedullary lipomas. AJR Am J Roentgenol 2000;174(6):1792–1793.
36. Falavigna A, Segatto AC, Salgado K. A rare case of intramedullary lipoma associated with cyst. Arq Neuropsiquiatr 2001;59(1):112–115.
37. Cools MJ, Al-Holou WN, Stetler WR Jr, et al. Filum terminale lipomas: imaging prevalence, natural history, and conus position. J Neurosurg Pediatr 2014;13(5):559–567.
38. Lotfinia I, Mahdkhah A. The cystic dilation of ventriculus terminalis with neurological symptoms: three case reports and a literature review. J Spinal Cord Med 2018;41(6):741–747.
39. Coleman LT, Zimmerman RA, Rorke LB. Ventriculus terminalis of the conus medullaris: MR findings in children. AJNR Am J Neuroradiol 1995;16(7):1421–1426.
40. Heuser CC, Hulinky RS, Jackson GM. Caudal Regression Syndrome. In: Copel JA, D'Alton ME, Feltovich H, et al, eds. Obstetric Imaging: Fetal Diagnosis and Care. 2nd ed. Philadelphia, Pa: Elsevier, 2018; 291–294.
41. Bell R, Glinianaia SV, Tennant PW, Bilous RW, Rankin J. Peri-conception hyperglycaemia and nephropathy are associated with risk of congenital anomaly in women with pre-existing diabetes: a population-based cohort study. Diabetologia 2012;55(4):936–947.
42. Lee SM, Cheon JE, Choi YH, et al. Limited Dorsal Myeloschisis and Congenital Dermal Sinus: Comparison of Clinical and MR Imaging Features. AJNR Am J Neuroradiol 2017;38(1):176–182.
43. Kim JW, Wang KC, Chong S, Kim SK, Lee JY. Limited Dorsal Myeloschisis: Reconsideration of its Embryological Origin. Neurosurgery 2020;86(1):93–100.

44. Pang D, Zovickian J, Wong ST, Hou YJ, Moes GS. Limited dorsal myeloschisis: a not-so-rare form of primary neurulation defect. Childs Nerv Syst 2013;29(9):1459–1484.
45. Pang D, Zovickian J, Oviedo A, Moes GS. Limited dorsal myeloschisis: a distinctive clinicopathological entity. Neurosurgery 2010;67(6):1555–1579; discussion 1579–1580.
46. Tortori-Donati P, Fondelli MP, Rossi A, Raybaud CA, Cama A, Capra V. Segmental spinal dysgenesis: neuroradiologic findings with clinical and embryologic correlation. AJNR Am J Neuroradiol 1999;20(3):445–456.
47. Emmanouilidou M, Chondromatidou S, Arvaniti M, Goutsaridou F, Papapostolou P, Tsitouridis I. Spinal segmental dysgenesis: presentation of a rare spinal congenital abnormality. Neuroradiol J 2008;21(3):388–392.
48. Chellathurai A, Ayyamperumal B, Thirumaran R, Kathirvelu G, Muthaiyan P, Kannappan S. Segmental Spinal Dysgenesis: "Redefined." Asian Spine J 2019;13(2):189–197.
49. Deora H, Srinivas D, Shukla D, et al. Multiple-site neural tube defects: embryogenesis with complete review of existing literature. Neurosurg Focus 2019;47(4):E18.
50. Ramdurg Shashank R, Shubhi D, Vishal K. Multiple neural tube defects: a rare combination of limited dorsal myeloschisis, diplomyelia with dorsal bony spur, sacral meningocoele, syringohydromyelia, and tethered cord. Childs Nerv Syst 2017;33(4):699–701.